Lattice enhanced Fano resonances from bound states in the continuum metasurfaces

*Thomas CW Tan, Eric Plum and Ranjan Singh **

((Optional Dedication))

T. CW. Tan, Prof. R. Singh
Division of Physics and Applied Physics, School of Physical and Mathematical Sciences,
Nanyang Technological University, Singapore 637371, Singapore
E-mail: ranjans@ntu.edu.sg

T. CW. Tan, Prof R. Singh
Centre for Disruptive Photonic Technologies, The Photonics Institute,
Nanyang Technological University, Singapore 637371, Singapore

Dr. E. Plum
Centre for Photonic Metamaterials & Optoelectronics Research Centre, Zepler Institute,
University of Southampton, Southampton, SO17 1BJ, UK

Keywords: bound state in the continuum, Fano resonance, metamaterials,
terahertz, lattice mode

Fano resonances in metamaterials are known for their high quality (*Q*) factor and high sensitivity to external perturbations, which makes them attractive for sensors, lasers, non-linear and slow light devices. However, Fano resonances with higher *Q* factors obtained through structural optimization of individual resonators are accompanied by lower resonance intensity, thereby limiting the overall figure of merit (*FoM*) of the resonance. This article reports a strategy for simultaneously enhancing the *Q* factor and *FoM* of Fano resonances in terahertz metamaterials. Coupling of the Fano resonance, which arises from a symmetry protected bound state in continuum, to the first order lattice mode of the metamaterial array leads to stronger field confinement and substantial enhancement of both *Q* factor and *FoM*. As such enhancement occurs in planar metamaterials independently of the resonator geometry, the proposed approach can be utilized for a wide range of high-*Q* and high-sensitivity terahertz metadevices.

Controlling losses in metamaterials to obtain narrow resonances is important for photonic applications such as sensors[1-3], low-power switches/modulators[4], and narrowband filters[5] across the electromagnetic spectrum. These losses can be non-radiative or radiative and both can be minimised by choosing favourable materials and an optimal metamaterial design. Since Drude metals have high conductivity at terahertz frequencies, free electrons in the conduction band of metals experience little resistive heating when interacting with THz radiation, resulting in low non-radiative energy losses in non-resonant metallic structures. Therefore, radiative losses are the main cause of loss in non-resonant metallic THz metamaterials, where the oscillating fields of free electrons easily couple to free space. In symmetric structures, the incident field excites an in-phase collective dipole excitation of free electrons, which re-radiates efficiently to the far field. However, a sharper resonance possessing a higher quality (Q) factor due to lower radiative losses can be realized by destructive interference of different excitations. Such interference between a broad spectral line or continuum and a discrete resonance state gives rise to Fano[6] resonances which are asymmetric in line shape. They were initially observed in quantum systems[7-10] and the classical analogue of this phenomenon is also observed in a variety of photonic systems, including metamaterials.[11-15]

Recently, Fano resonances of metasurfaces have been linked to bound states in continuum (BIC), which is a field of growing interest. BICs are bound eigenmodes which lie above the photonics light line.[16-20] This itself is a unique counterintuitive characteristic and because of this, they possess infinite lifetimes and zero-linewidth resonances under ideal conditions.[21-24] However, in the real world, ideal conditions are not possible, and therefore the investigation of a quasi-BIC (QBIC) is the only way to study BIC phenomena. In this context, the QBIC is a point where the symmetry protected BIC collapses, resulting in loss of its infinite lifetime and zero linewidth. Hence the characteristics of QBIC include an extremely narrow linewidth which leads to an ultra-high Q factor. The small, but non-zero, losses of metals at THz frequencies

prevent the realization of BIC and limit their QBIC approximations, but instead Fano resonances can be observed easily. The link between the two, BIC and Fano resonance, is that both phenomena are a result of destructive interference coupling. Therefore, methods that enhance Fano resonances to approach QBIC states with ultra-high *Q* factors could yield ultra-low-loss metallic metamaterial devices, as well as detectors with the resolution to pick up these narrow resonances.[25]

Metamaterials consist of periodic subwavelength structures that can be engineered to support a resonant response to the incident electromagnetic wave. Depending on the geometry and coupling of the metamaterial structures, a wide range of resonances can be excited.[13, 14, 26-30]. Fano resonances in metamaterial structures are realized through symmetry breaking and can be described in terms of interactions between bright and dark modes.[13] The bright mode is excited by the incident light and is highly radiative, while the dark mode is subradiant and is only accessible through the near field excitation by the bright mode. In metamaterials, the Fano lineshape can be optimised by decreasing the structural asymmetry of the resonator to give a sharp spectral response (high *Q* factor). However, such *Q* factor optimisation often leads to low resonance intensity (*I*) and limits the maximum figure of merit ($FoM = Q \times I$).[12] Here, we show an approach to improve both *Q* factor and Figure of Merit by coupling the plasmonic resonance[31-35] to the first order lattice mode that is inherent in any periodic subwavelength system. The lattice modes arise from the collective Rayleigh scattering of periodic structures, where energy is strongly concentrated on the surface that fails to radiate to the far-field. Hence, coupling a lattice mode with a resonance of a metamaterial can reduce the resonance's radiative losses, resulting in an enhancement of its *Q*-factor.[36-38] The resonance frequencies of the lattice modes are determined by the refractive index of the material and lattice period of the metamaterial array. Therefore, by changing the lattice period of the structure, a lattice mode

can be easily adjusted to couple to a plasmonic structural resonance to achieve *Q* factor enhancement.

In this article, we experimentally study the coupling of the Fano resonance of an asymmetric split ring resonator (ASRR) to the first order lattice mode (FOLM) of the resonator array. Previous studies have shown enhanced *Q* factors by coupling a lattice mode to inductive-capacitive (LC) resonances[39-41] and electromagnetically-induced-transparency-type (EIT-type)[40, 42-46] resonances. Here, we demonstrate FOLM coupling to a Fano resonance obtained through magnetic coupling and observed both *Q* factor and *FoM* enhancement. The ASRR was designed to support a Fano resonance at about 1 THz and a dipole resonance at a lower frequency of 0.853 THz. Compared to a conventional square ASRR consisting of two end-coupled resonator arms, this was achieved by *flipping* the resonator arms resulting in an ASRR consisting of side-coupled resonator arms. The coupling nature of the ASRR is determined by analysing the electric and magnetic dipole moments of the transversely coupled resonator arms, which determines the symmetric and antisymmetric coupled modes represented by the higher and lower frequency split modes.[47] Lattice mode coupling is achieved by tuning the lattice mode frequency f_{LM}. At normal incidence,

$$f_{\mathrm{LM}} = \frac{c}{nP}\sqrt{i^2 + j^2} \qquad (1)$$

where *c* is the speed of light in vacuum, *n* is the refractive index of the medium where the lattice mode propagates, *P* is the periodicity of the square lattice and (*i*, *j*) are indices defining the order of the lattice mode. For this investigation, the first order lattice mode (FOLM) (0,1) – that propagates in the metamaterial's silicon substrate – is used to interact with the metamaterial resonances. In the frequency ranges considered here, the metamaterials do not diffract in air. As the FOLM traps most of the THz energy on the surface of the metamaterial array, it strengthens the resonant near-field confinement of the metamaterial resonance.[48, 49] After the

investigation of lattice coupling, angle-dependent simulations were performed on a symmetric resonator under ideal conditions to determine the nature of the Fano resonance. Our findings demonstrate the evolution of a BIC to a Fano resonance. Since an ideal BIC cannot be realized, one way of observing this phenomenon experimentally at normal incidence is to induce a QBIC through symmetry breaking of the resonators, which is well-known to lead to Fano resonances. An ideal BIC, characterized by infinite lifetime (infinite *Q* factor), is divergent in nature, however, it decreases to a finite quantity in response to any perturbation that breaks the in-plane symmetry, i.e. any illumination angle[50] or structural parameter that makes the excitation of one resonator arm distinguishable from the other. Thus, we investigate whether real world parameters of Fano resonance coupling and enhancement with the FOLM could achieve a QBIC state.

The split modes excited in a typical asymmetric split ring resonator consist of a low frequency Fano resonance and a higher frequency dipole resonance.[2, 12, 29, 42, 51, 52] The Fano resonance being the lower frequency split mode implies that coupling to the lattice mode would require a sparse array (large period), which may be inefficient. Therefore, the coupling of the ASRR was changed from capacitive coupling to inductive coupling by flipping the arms of the ASRR, as shown in the insets of **Figure 1**. The nature of coupling between the resonator arms determines the resonance frequency of the Fano resonance, which can be lower [Figure 1(a)] or higher [Figure 1(b)] than the frequency of the dipole resonance. Fano resonances in such metamaterials are characterized by anti-parallel surface currents as shown in insets of Figure 1(a) for a square ASRR and Figure 1(b) for the flipped ASRR. This brings the Fano resonance closer to the first order lattice mode frequency (cyan dotted line), which allows for efficient resonance coupling.

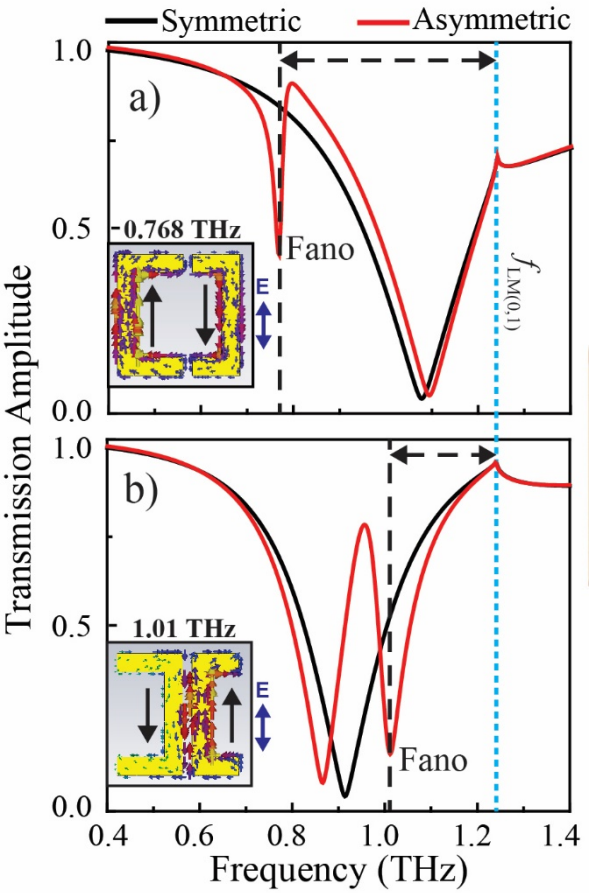

Figure 1. Fano resonances of different aluminum resonator configurations. (a) Square configuration of end-coupled resonator arms and (b) side-coupled configuration with the resonating arms flipped. Simulations of the Fano resonance excitation allowed by asymmetry resulting from displacement of the gap by a distance d = 3 µm from the central (symmetric) position while maintaining overall dimensions of 40 µm × 40 µm, an arm width of 6 µm, a gap of $g = 3$ µm and a period of 70 µm. The insets show the simulated surface currents at the transmission minimum of the Fano resonances at (a) 0.768 THz and (b) 1.01 THz. A cyan dotted line marks the first order lattice mode $f_{LM(0,1)}$.

The ASRR shown in the inset of **Figure 2**(a) has a size of 40 × 40 µm^2, an arm width of 6 µm and a gap of 3 µm. The gap is displaced by $d = 3$ µm from the central vertical axis of the resonator to break the symmetry of the system and the incident radiation is polarized with the electric field parallel to the vertical axis (*y*-polarized). To emphasize its physical significance, we refer to the gap as the coupling distance g between the split arms. To show the change from capacitive to inductive coupling, the coupling distance is varied as shown in Figure 2(b). The figure shows a blue shift of a transparency peak for decreasing coupling distances, $g = 9, 5, 3$ µm, where the asymmetry used is d =1 µm for a lower transparency peak strength, as this

makes the tuning of the transparency peak more visible. The blue shift of the transparency peak changes the Fano resonance from being the lower frequency split mode to the higher frequency split mode, where $g = 5$ is the threshold position when the transparency peak is exactly at the centre of the broad resonance dip. The switch from capacitive to inductive coupling can be seen in either the electric dipole (*p)* or the magnetic dipole (*μ)* moments of each arm of the ASRR obtained from simulated surface currents at the resonance frequencies of the transmission spectrum. Only transverse coupling is relevant for *y*-polarized ASRR illumination, which is considered here. Transverse coupling of an antisymmetric mode results in an attractive force that decreases the restoring force, and controls the resonant charge oscillation, leading to a lower resonance frequency. In contrast, transverse coupling of a symmetric mode results in repulsion that increases the restoring force, leading to a higher resonance frequency.[47] At $g = 9$ μm, the dominant coupling is electric as the lower frequency split mode (Fano resonance) corresponds to the transverse coupling of electric dipoles aligned anti-symmetrically, whereas the higher frequency mode corresponds to the symmetric transverse coupling of electric dipole moments, as shown in Figure 2(b-i) and (b-ii), respectively. This transmission spectrum is similar to that of a typical ASRR (without flipped resonator arms) as shown in Figure 1(a), where the Fano resonance is also the lower frequency split mode. At a coupling distance of $g = 3$, the dominant transverse coupling is magnetic, where the Fano resonance is now the higher frequency split mode which corresponds to magnetic dipoles aligned symmetrically, while the lower frequency split mode corresponds to antisymmetric coupling of magnetic dipoles. Though the coupling is revealed by the relative orientations of the resonant electric or magnetic dipole moments and the spectral position of the corresponding transmission resonances, the Fano resonance is still represented by antisymmetric surface currents [Figure 2(b-i) and (b-vi)], which trap energy in the resonators as emission from both resonator arms is prevented by destructive interference in the far field.

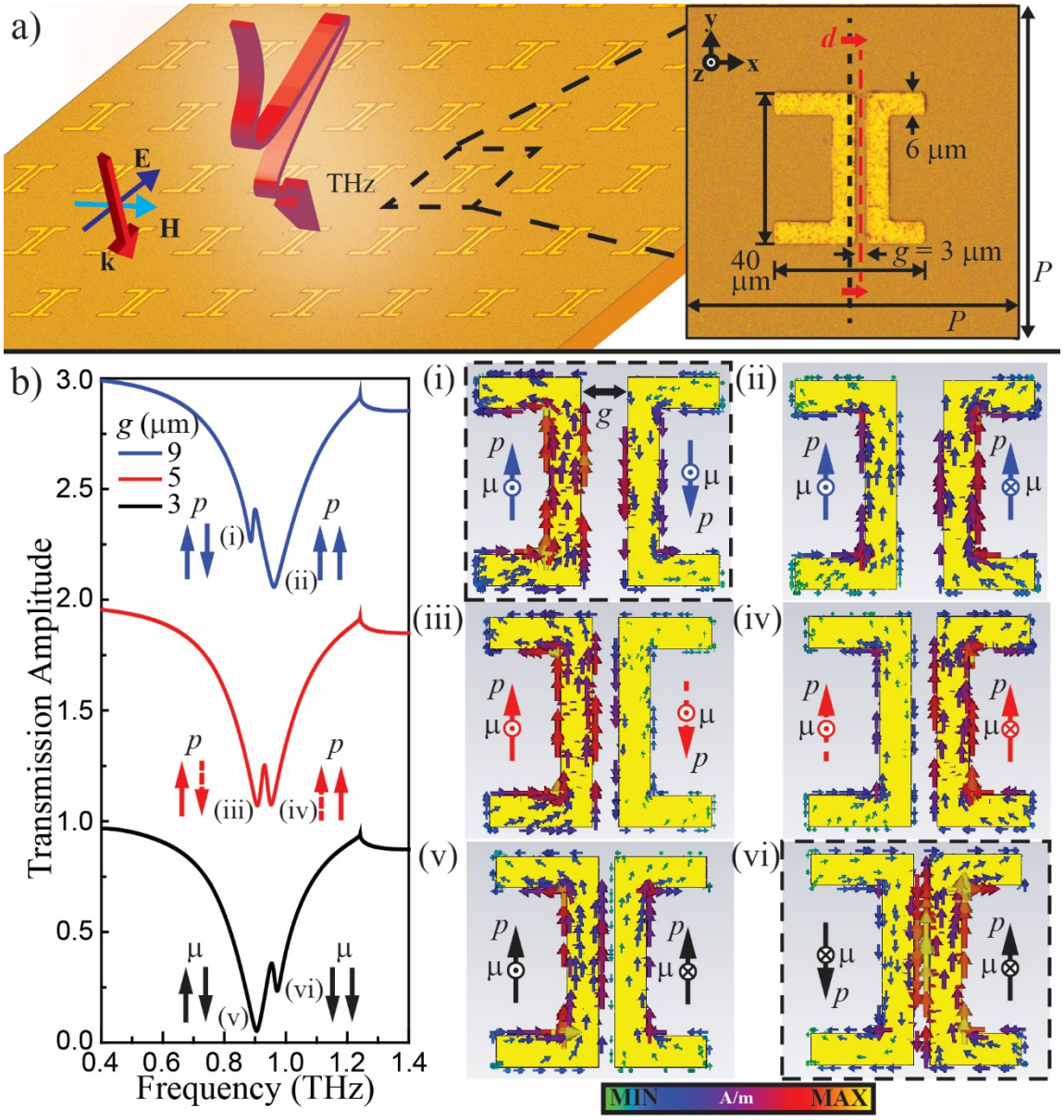

Figure 2. Fano-metamaterial. (a) Optical microscope image of the metamaterial array with schematic illustration of the incident THz field. The inset shows a unit cell containing an asymmetric split ring resonator. (b) Simulated transmission amplitude of aluminum asymmetric split ring resonators with $P = 70$ μm period, $d = 1$ μm asymmetry and coupling distances of $g = 9,\ 5$ and 3 μm. Their resonances are labelled (i)-(vi) and the corresponding surface currents, electric dipole moments (p) and magnetic dipole moments (μ) are shown.

Metamaterial samples were fabricated on a high resistivity ($\rho > 5000\ \Omega \cdot \mathrm{cm}$) silicon substrate of 500 μm thickness. The samples were patterned using conventional photolithography, followed by thermal evaporation of 200-nm-thick aluminum metal and a lift off process leaving behind the resonator array, as shown in Figure 2(a). The fabricated metamaterial samples were measured using a terahertz time-domain spectroscopy system to characterize their transmission

properties. For the excitation of the Fano resonance, a *y*-polarized terahertz beam illuminates the sample at normal incidence. The transmission amplitude is calculated as $t(\omega) = |E_s(\omega)/E_r(\omega)|$, where subscripts *s* and *r* correspond to the Fourier transforms of the time-domain electric field transmitted through the sample and a reference substrate, respectively.

We studied the interaction between the FOLM and the metamaterial resonances of the ASRR both numerically and experimentally. Numerical investigations were conducted using a commercially available frequency-domain solver based on the finite-difference time-domain (FDTD) method, *Computer Simulation Technology* (CST) *Microwave Studio*. The refractive index of the silicon substrate and the conductivity of aluminium were modelled as $n = 3.42$ and $\sigma = 3.56 \times 10^7 \mathrm{S/m}$, respectively. The simulated and measured transmission spectra of the ASRR arrays of varying period (*P*) are shown in **Figure 3**. The spectra show the dipole and Fano resonances around 0.8 THz and 1.0 THz, respectively. For a lattice period of *P* = 75 μm, the FOLM that is indicated by the cyan dotted line/arrow occurs at a frequency of 1.16 THz, which is higher than the Fano resonance frequency. Increasing the lattice period decreases the lattice mode resonance frequency and allows it to couple to the metamaterial resonances. Resonant coupling between the lattice mode and the Fano resonance is observed as the lattice period is increased from 75 μm to 90 μm [Figure 3(a-d)]. We see a narrowing of the Fano resonance as the lattice mode (cyan dotted line) approaches the Fano resonance with increasing lattice period. When the lattice mode frequency matches the Fano resonance at *P* = 90 μm [Figure 3(d)], the Fano resonance is of the narrowest linewidth. Increasing the lattice period further (*P* > 90 μm) decreases the lattice mode frequency, causing a frequency mismatch between the FOLM and the Fano resonance. This decreases the strength of the Fano resonance and broadens its linewidth. Similar behaviour is observed for the dipole resonance when the lattice period is increased such that the lattice mode frequency approaches and couples to the dipole resonance frequency for periods from *P* = 110 μm to 118 μm [Figure 3(e-g)]. The

transmission minimum of the dipole resonance is narrowest when the lattice mode frequency matches the dipole resonance at P = 118 μm [Figure 3(g)]. As the lattice period is increased further to P > 118 μm, there is a frequency mismatch between the lattice mode and the dipole resonance and hence the resonances gradually decouple, thereby weakening the resonance strength, as seen in Figure 3(h) at P = 122 μm. We note that the (1,1) lattice mode couples to the Fano resonance as the lattice period approaches P = 122 μm and a linewidth narrowing can also be seen in this case. Simulations and experiments are in good qualitative agreement. Quantitative differences regarding linewidth and strength of resonances are mainly due to limited resolution of the experimental setup (~30 GHz), which is unable to resolve ultra-narrow resonances.

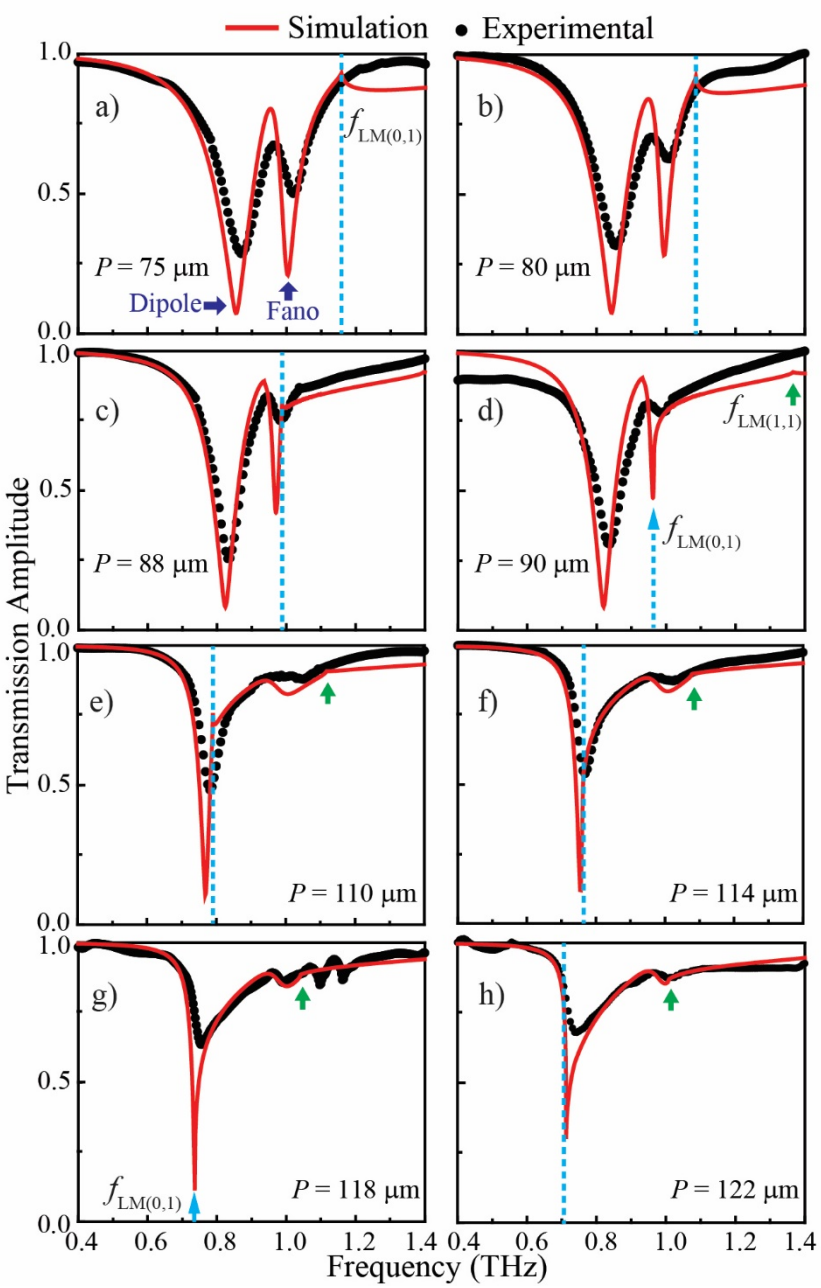

Figure 3. Coupling resonances of aluminum split rings and lattice. Simulated and measured transmission amplitude of metamaterials with asymmetry $d = 3$ μm, coupling distance $g = 3$ μm and lattice periods from P = 75 to 122 μm. (a – d) Narrowing of the Fano resonance and (e – h) narrowing of the dipole resonance due to interaction with a lattice mode. Cyan dotted lines/arrows indicate the first order lattice mode (0,1), while green arrows indicate the (1,1) order lattice mode. Critical periods are 90 μm and 118 μm, where the (0,1) lattice mode frequency matches the metamaterial's Fano and dipole resonances, respectively.

Narrow resonance features are quantitatively described by the Q factor, estimated by $Q = \omega_0/\Delta\omega$, where $\Delta\omega$ is the full width at half maximum (FWHM) of the resonance intensity and ω_0 is the resonance frequency. These resonance parameters are obtained from the transmittance

spectrum, $T(\omega) = |t(\omega)|^2$, using the following equation that describes the Fano resonance[6, 53],

$$T(\omega) = T_0 + H\frac{(W+q)^2}{(1+q^2)(1+W^2)}, W = \frac{\omega-\omega_0}{\Delta\omega/2} \quad (2)$$

where T_0 and H are constants, q is the asymmetry parameter which determines the resonance profile while W is a normalized expression containing the resonance frequency ω_0 and the FWHM $\Delta\omega$. The Q factor also directly relates to the losses in the metamaterial system, which can be radiative or non-radiative. But as discussed above, the losses are mainly radiative as Drude metals have high conductivity at terahertz frequencies. A common characteristic in metamaterial Fano resonances is that high-Q Fano resonances have a low intensity (transmission change) and higher intensity resonances have a lower Q. A high intensity Fano resonance at low asymmetric displacement (d = 3 μm) was used to show the effect of lattice mode coupling. We note that a higher Q factor of the Fano resonance could be achieved by optimizing the ASRR asymmetry, however, such "optimization" would disregard the practical importance of resonances that are not only narrow but that also exhibit a large resonance amplitude. In order to simultaneously optimize both resonance width and resonance depth, we consider a Figure of Merit (*FoM*) defined as $FoM = Q \times I$, where Q is the resonance Q factor and I is the resonant transmission change in terms of intensity. **Figure 4**(a,b) shows the Q factor and *FoM* as the period of the metamaterial unit cell increases, tuning the lattice mode frequency relative to the metamaterial resonances. From P = 70 μm to 90 μm, the Fano resonance Q factor increases gradually and upon reaching the critical period for Fano coupling $P_c^{\mathrm{Fano}} = 90$ μm, it reaches a maximum of 59. A minor increase of Q factor is seen for the dipole resonance at P = 70 μm to 90 μm, but it increases significantly at P > 90 μm, to a maximum of 19 at P = 114 μm. Interestingly, the lattice mode resonantly couples to the dipole resonance at $P_c^{\mathrm{dipole}} = 118$ μm but its maximum Q factor was obtained at P = 114 μm. This is because the resonance interaction occurs near the half maximum of the high-intensity dipole resonance for P = 114

μm and at its transmission minimum for P = 118 μm, resulting in squeezing of FWHM and tip of the dipole resonance, respectively. Therefore, the Q factor at P = 114 μm is slightly higher than at the critical period, $P_c^{dipole} = 118$ μm. A similar trend is seen for the *FoM*, which also increases with increasing lattice period as the lattice mode frequency approaches the metamaterial resonances, reaching a maximum value of *FoM* = 33 for the Fano resonance at $P_c^{Fano} = 90$ μm and a maximum of *FoM* = 15 for the dipole resonance at P = 114 μm. Figure 4(c) shows the simulated transmission amplitude spectra as a function of the lattice period. It clearly depicts the resonance narrowing as the lattice mode approaches and then matches the ASRR Fano and dipole resonance frequencies at the critical periods of 90 and 118 μm.

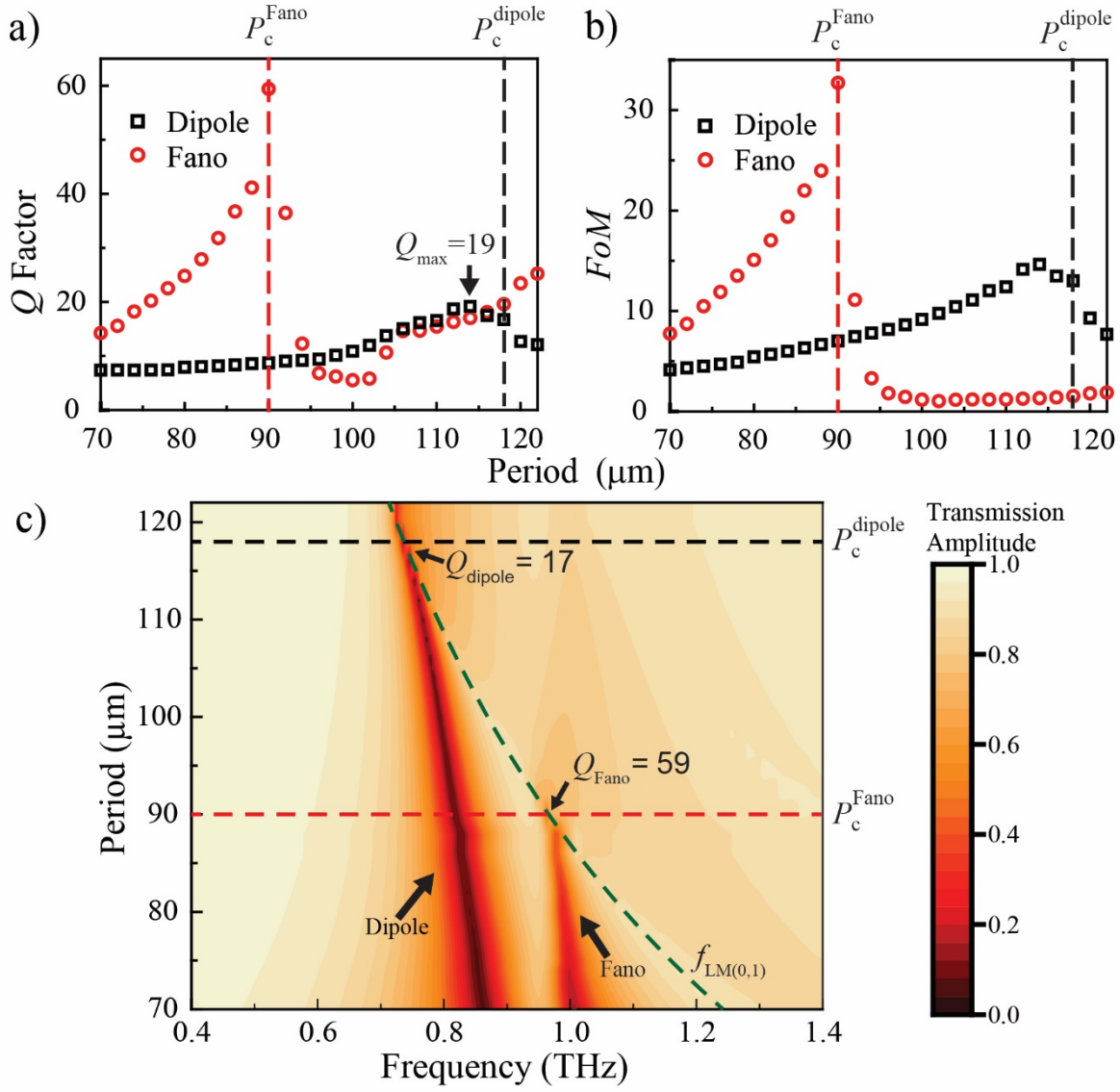

Figure 4. Lattice-dependence of resonant metamaterial properties extracted from simulations. (a) Q factor and (b) figure of merit ($FoM = Q \times I$, with resonant transmission intensity change I) of the dipole (black) and Fano (red) resonances at different lattice periods of the aluminum metamaterial with asymmetry $d = 3$ μm and coupling distance $g = 3$ μm. (c) Transmission amplitude as a function of the metamaterial's period and frequency of the incident THz wave. The metamaterial resonances are narrowest when they coincide approximately with the lattice mode $f_{\mathrm{LM}(0,1)}$ for critical periods $P_{\mathrm{c}}^{\mathrm{Fano}} = 90$ μm and $P_{\mathrm{c}}^{\mathrm{dipole}} = 118$ μm (dashed lines).

To determine the nature of the Fano resonance and the ability of its enhancement due to FOLM coupling to achieve a QBIC state under realistic parameters, an illumination-angle-dependent simulation is performed assuming ideal metallic resonators made from perfect electric conductor (PEC). **Figure 5**(a) shows the transmission amplitude as a function of illumination angle and frequency for arrays of symmetric ($d = 0$) PEC metamaterial resonators with coupling distances of $g = 3, 5$ and 9 μm and otherwise of the same geometry as in Figure 2. Similar to Figure 2(b), the coupling distance determines the coupling nature (magnetic or electric) of the metamaterial and hence the spectral positions of the dipole resonance, the BIC/QBIC/Fano resonance and the transmission peak in between. As the angle of incidence increases, we can see the collapse of the symmetry protected BIC at normal incidence to a resonance with a finite linewidth, at 0.97, 0.93 and 0.90 THz for $g = 3, 5$ and 9 μm respectively (red arrows in Figure 5(a)). The QBIC state is where the BIC just collapses and loses its zero linewidth and infinite lifetime. This happens at a slight perturbation of the symmetry protected system as illustrated by Figure 5(b), where we see the QBIC with an ultra-narrow linewidth for 2° oblique illumination of the symmetric PEC structure (black lines). To facilitate measurements at normal incidence, another method to induce a QBIC resonance is to break the structural symmetry of the resonator. This is illustrated by Figure 5(b) for normal illumination of PEC ASRR arrays, where the gaps are displaced from the resonator's central vertical axis by the asymmetry parameter d = 0.25 μm (red dashed lines). Both BIC perturbations, either a small illumination angle or a small structural asymmetry, yield QBIC at

almost identical spectral positions [Figure 5(b)] and similar behaviour has also been reported by other groups.[22-24] Figure 5 also illustrates that the QBIC can be tuned across the broad continuum by changing the coupling distance between the components of the metamaterial unit cell, from high frequencies to an EIT-like spectrum and low frequencies.

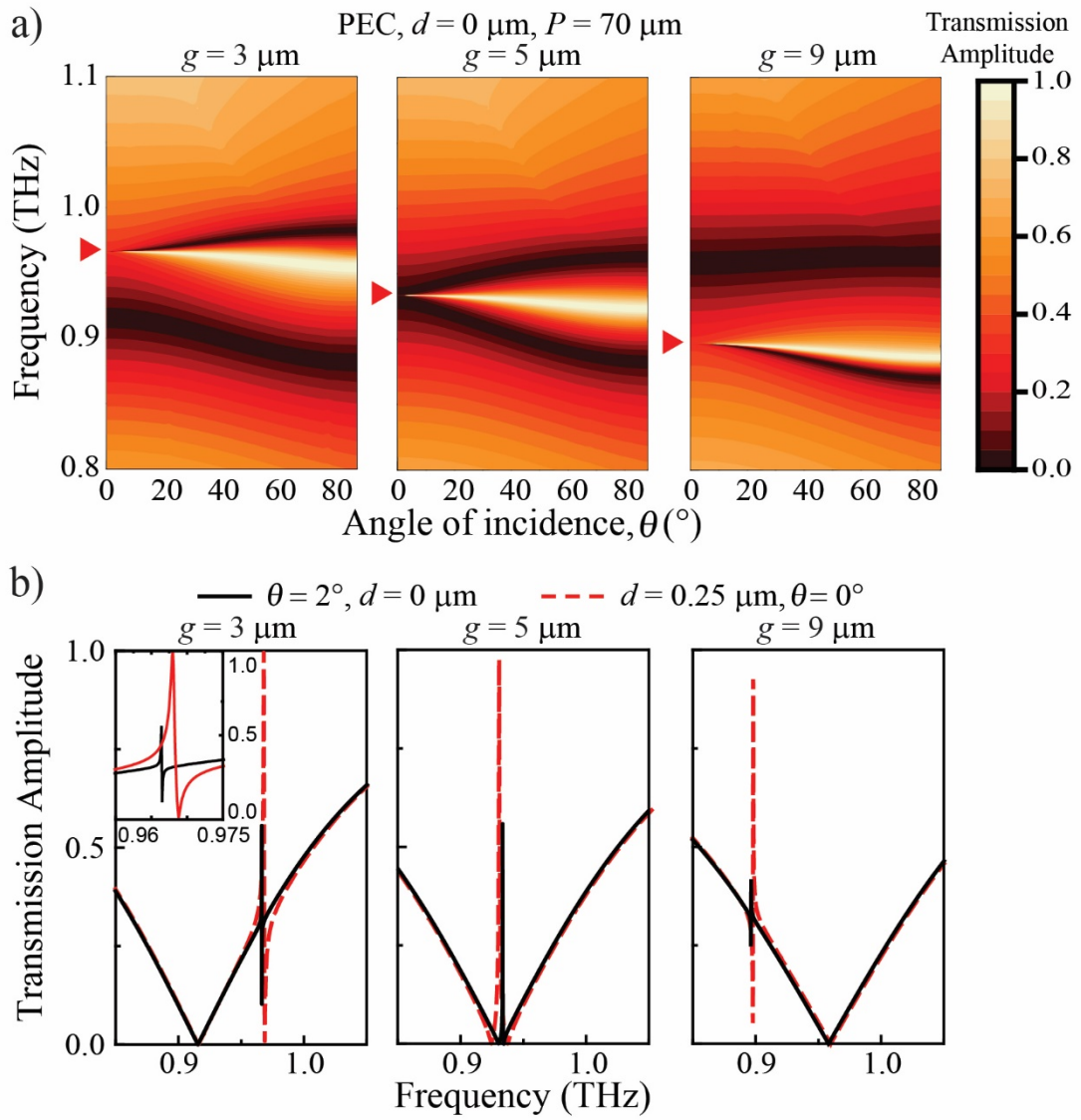

Figure 5. Excitation of bound metamaterial states in the continuum by symmetry breaking. Simulations are shown for metamaterial arrays with period P = 70 µm consisting of PEC resonators with different coupling distances of $g = 3, 5$ and 9 µm. (a) Transmission amplitude spectra of symmetrically coupled resonators ($d = 0$ µm) as a function of angle of incidence in the *xz*-plane. Symmetry protected BIC are shown by red arrows at normal incidence. (b) Transmission amplitude spectra of QBIC excited by illumination of the symmetric structures with 2° angle of incidence (solid lines) or at normal incidence by introduction of a small structural asymmetry $d = 0.25$ µm (dashed lines). An example of the ultra-narrow resonance of the QBIC is shown and magnified in the inset of $g = 3$ µm.

As the perturbation is reduced towards zero to approach the symmetry-protected BIC, the line width becomes zero and the *Q* factor diverges to infinity, as shown in **Figure 6**. Our simulations show that both oblique illumination of symmetric resonators [Figure 6(a)] and structural asymmetry of resonators at normal incidence [Figure 6(b)] can control the *Q* factor of QBIC/Fano resonances in PEC metamaterials by at least two orders of magnitude. While the *Q* factor could in principle diverge to infinity under ideal conditions, under real world conditions, losses and detector resolution limit the achievable and detectable *Q* factors. This effect of losses is shown for aluminium resonator arrays with a coupling distance $g = 3$ μm, which achieved maximum *Q* factors that are about two orders of magnitude lower than those calculated for PEC resonator arrays. For these aluminium resonator arrays, the highest *Q* factor resonances, that occur at near-normal incidence [Figure 6(a)] / low asymmetry [Figure 6(b)], suffer from low resonance intensity. Figure 6(c) shows a comparison of *Q* factors between arrays of PEC and aluminium ASRRs with asymmetry $d = 3$ μm and coupling distance $g = 3$ μm for different lattice periods, where FOLM coupling and enhancement of the Fano/QBIC resonance occurs at P = 89 and 90 μm for PEC and aluminium ASRRs, respectively. While FOLM coupling enhances the *Q* factor, the maximum *Q* factor calculated with FOLM coupling under real world conditions is still about two orders of magnitude lower than that of the QBIC under ideal low-asymmetry PEC conditions. For aluminium resonators, our results indicate that the three different optimization strategies – small angle of incidence onto symmetric resonators, normal incidence onto low-asymmetry resonators and FOLM coupling – yield comparable maximum Q-factors, which are limited by non-radiative losses in aluminium. We note that the resonators used for FOLM coupling have a significant asymmetry of $d = 3$ μm – and thus high resonance intensity – for experimental detection and suffer from ohmic losses in the metal as well as a small amount of substrate absorption. Very low asymmetry resonators made from low-loss materials will require high fabrication accuracy to avoid inhomogeneous broadening and

precise matching of the FOLM to the ultra-narrow Fano/QBIC resonance to achieve resonance enhancement.

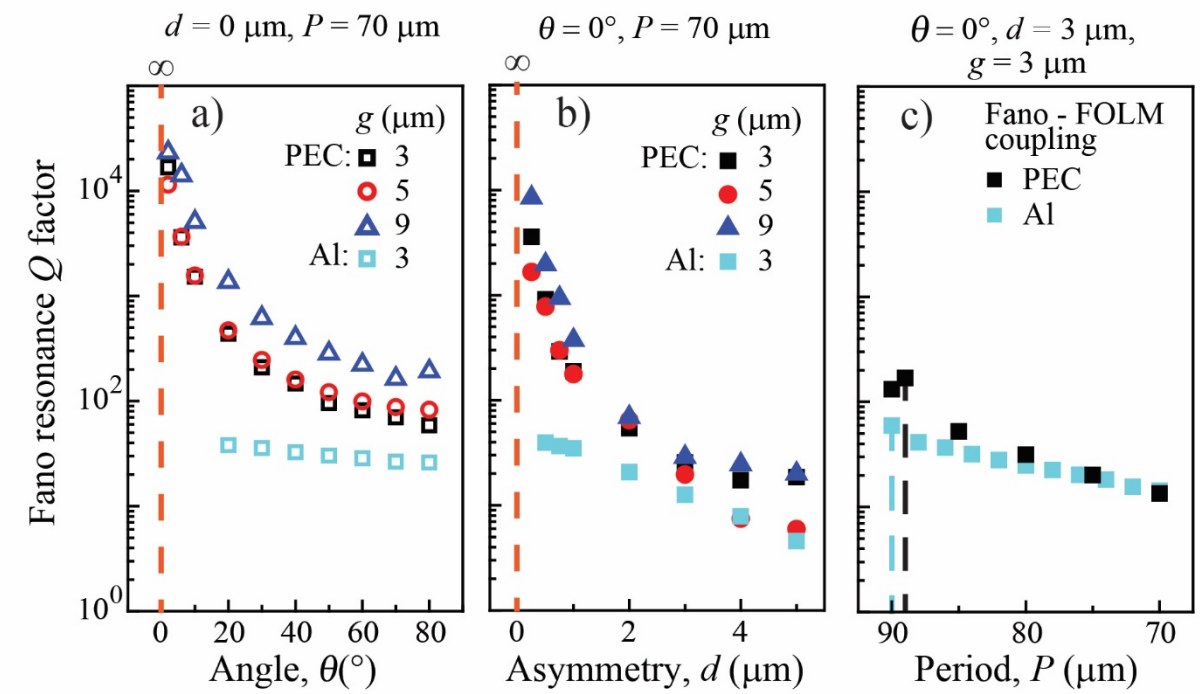

Figure 6. *Q* factor of the simulated Fano resonance as a function of (a) angle of incidence θ, (b) asymmetry d and (c) period P. (a, b) The Q factor of PEC resonator arrays diverges to infinity when incidence angle and asymmetry both approach 0 as the resonance is protected by symmetry in this case. Results for aluminum resonator arrays with a coupling distance of $g = 3$ μm are shown for comparison. (c) Comparison between ideal PEC and realistic aluminum resonator arrays with asymmetry $d = 3$ μm and coupling distance $g = 3$ μm for different periods, where FOLM coupling is indicated by a dashed line.

To further investigate the Q factor enhancement of the metamaterial resonances due to FOLM coupling, we performed numerical simulations of the electric and magnetic field under lattice matched and mismatched conditions of both the Fano and dipole resonances. **Figure 7**(a-d) shows the electromagnetic field distributions of the Fano resonance mismatched and matched to the first order lattice mode at P = 70 and 90 μm, respectively. Under lattice matched conditions we observe some electric field enhancement on the ends of the left resonator arm and along the gap. Since the Fano resonance arises from the inductively coupled resonator arms, we also see a strong enhancement of the magnetic fields in the gap. This enhancement due to coupling to the lattice mode strengthens the confined light in the gap and the FOLM-enhanced fields are evidence of reduced radiative losses, leading to the high Q lattice matched

metamaterial resonance. Figure 7(e-h) shows the electromagnetic field distribution of the dipole resonance mismatched and matched to the first order lattice mode at P = 70 µm and P = 118 µm. Similar results can be seen in the fields of the dipole resonance, where lattice matching yields stronger overall excitation of the structure. While only the longer resonator arm is strongly excited without lattice matching, FOLM-coupling of the dipole resonance at P = 118 µm results in substantial excitation of both resonator arms. Magnetic field enhancement due to lattice-matching is seen along the inner edge of each C-shaped resonator arm, which is evidence of increased currents in each resonator arm. However, the magnetic field within the gap between the resonator arms remains weak, and indeed the magnetic fields generated by a pair of identical electric dipoles is expected to cancel here.

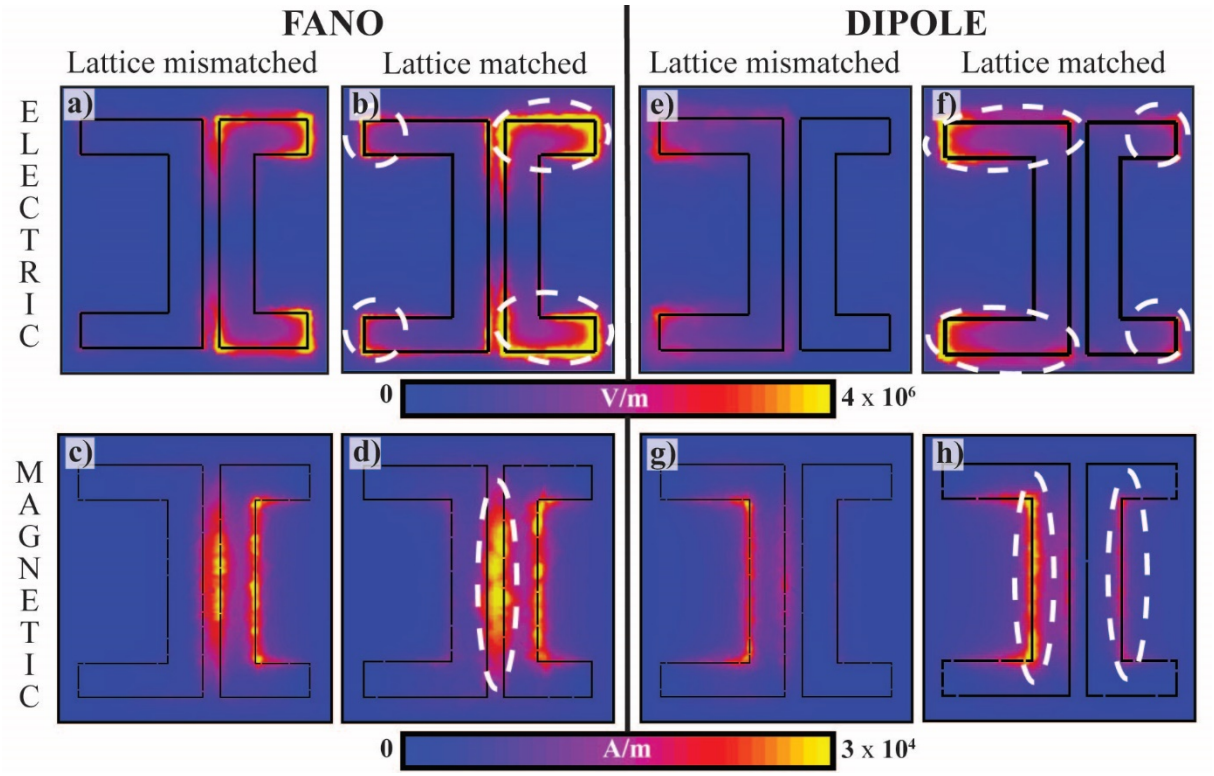

Figure 7. Lattice-induced field-enhancement. The near field total electric and magnetic field amplitude, |E| and |B|, of the Fano and dipole resonance under lattice mismatched (P = 70 µm) and lattice matched conditions (Fano: P = 90 µm; dipole: P = 118 µm) for aluminum split ring arrays with asymmetry $d = 3$ µm and coupling distance $g = 3$ µm. All maps of the same field share a color scale with the same range. Field enhancement is marked by white dashed ovals under lattice matched conditions.

In summary, lattice mode matching was performed on a terahertz asymmetric resonator with a Fano resonance as the higher frequency split mode. This was done by transverse coupling of symmetric magnetic dipole moments. The lattice mode traps electromagnetic fields in the plane of the metamaterial array and interferes with the metamaterial response, strengthening the resonant field confinement and reducing radiative loss. This lowered radiative loss yields a higher *Q* factor resonance. Here, lattice mode coupling increases the *Q* factor and Figure of Merit of the Fano transmission resonance by several times. We have shown that the Fano resonance originates from a symmetry protected BIC and radiates as a quasi-BIC state. We have shown that such quasi-BIC/Fano resonances can be tuned across the broad dipolar continuum by changing the coupling distance of the resonators. Coupling to the first order lattice mode provides a simple and general method for increasing the *Q* factor of metamaterial resonances for applications such as sensing, narrow band filtering and lasing spasers. The narrow gaps in this high frequency Fano design could also be used as micro channels for microfluidic sensing type applications.

Supporting Information

Supporting Information is available from the Wiley Online Library or from the author.

Acknowledgements

T.CW.T conceived the idea with the guidance of R.S and E.P. T.CW.T performed the simulations and experiments. T.CW.T wrote the manuscript with inputs from all authors. R.S and E.P supervised and revised the article. The author would also like to thank Manukumara Manjappa for discussions of this idea and Yogesh Kumar Srivastava for assisting in the fabrication.

The authors acknowledge funding support from Singapore's Ministry of Education (MOE) (Grant No. MOE2016-T3-1-006 and MOE2017-T2-1-110) and the UK's Engineering and Physical Sciences Research Council (Grant EP/M009122/1). The data from this paper is

Received: ((will be filled in by the editorial staff))
Revised: ((will be filled in by the editorial staff))
Published online: ((will be filled in by the editorial staff))

References

[1] X. Chen, W. Fan, Scientific Reports 2017, 7, 2092.
[2] R. Singh, W. Cao, I. Al-Naib, L. Cong, W. Withayachumnankul, W. Zhang, Applied Physics Letters 2014, 105, 171101.
[3] S. Yang, C. Tang, Z. Liu, B. Wang, C. Wang, J. Li, L. Wang, C. Gu, Optics Express 2017, 25, 15938.
[4] K. Nozaki, A. Shinya, S. Matsuo, T. Sato, E. Kuramochi, M. Notomi, Optics Express 2013, 21, 11877.
[5] M. Tonouchi, Nature Photonics 2007, 1, 97.
[6] U. Fano, Phys. Rev. 1961, 124, 1866.
[7] D. A. Broido, L. J. Sham, Physical Review B 1986, 34, 3917.
[8] J. Faist, F. Capasso, C. Sirtori, K. W. West, L. N. Pfeiffer, Nature 1997, 390, 589.
[9] D. Y. Oberli, G. Böhm, G. Weimann, J. A. Brum, Physical Review B 1994, 49, 5757.
[10] A. R. K. Willcox, D. M. Whittaker, Superlattices and Microstructures 1994, 16, 59.
[11] J. B. Pendry, A. J. Holden, D. J. Robbins, W. J. Stewart, IEEE Transactions on Microwave Theory and Techniques 1999, 47, 2075.
[12] L. Cong, M. Manjappa, N. Xu, I. Al-Naib, W. Zhang, R. Singh, Advanced Optical Materials 2015, 3, 1537.
[13] V. A. Fedotov, M. Rose, S. L. Prosvirnin, N. Papasimakis, N. I. Zheludev, Physical Review Letters 2007, 99, 147401.
[14] B. Luk'yanchuk, N. I. Zheludev, S. A. Maier, N. J. Halas, P. Nordlander, H. Giessen, C. T. Chong, Nature Materials 2010, 9, 707.
[15] S. D. Jenkins, J. Ruostekoski, N. Papasimakis, S. Savo, N. I. Zheludev, Physical Review Letters 2017, 119, 053901.
[16] E. N. Bulgakov, A. F. Sadreev, Physical Review A 2015, 92, 023816.
[17] C. W. Hsu, B. Zhen, J. Lee, S.-L. Chua, S. G. Johnson, J. D. Joannopoulos, M. Soljačić, Nature 2013, 499, 188.
[18] C. W. Hsu, B. Zhen, A. D. Stone, J. D. Joannopoulos, M. Soljačić, Nature Reviews Materials 2016, 1, 16048.
[19] B. Zhen, C. W. Hsu, L. Lu, A. D. Stone, M. Soljačić, Physical Review Letters 2014, 113, 257401.
[20] S. Han, L. Cong, Y. K. Srivastava, B. Qiang, M. V. Rybin, A. Kumar, R. Jain, W. X. Lim, V. G. Achanta, S. S. Prabhu, Q. J. Wang, Y. S. Kivshar, R. Singh, Advanced Materials 2019, 31, 1901921.
[21] A. A. Bogdanov, K. L. Koshelev, P. V. Kapitanova, M. V. Rybin, S. A. Gladyshev, Z. F. Sadrieva, K. B. Samusev, Y. S. Kivshar, M. F. Limonov, Advanced Photonics 2019, 1(1), 016001.
[22] K. Koshelev, S. Lepeshov, M. Liu, A. Bogdanov, Y. Kivshar, Physical Review Letters 2018, 121, 193903.
[23] L. Cong, R. Singh, Advanced Optical Materials 2019, 7, 1900383.
[24] D. R. Abujetas, N. van Hoof, S. ter Huurne, J. Gómez Rivas, J. A. Sánchez-Gil, Optica 2019, 6, 996.

[25] Y. K. Srivastava, R. Tanyi Ako, M. Gupta, M. Bhaskaran, S. Sriram, R. Singh, in *arXiv:1908.03662*, 2019.
[26] T. Koschny, P. Markoš, D. R. Smith, C. M. Soukoulis, Physical Review E 2003, 68, 065602.
[27] S. Linden, C. Enkrich, M. Wegener, J. Zhou, T. Koschny, C. M. Soukoulis, Science 2004, 306, 1351.
[28] W. J. Padilla, M. T. Aronsson, C. Highstrete, M. Lee, A. J. Taylor, R. D. Averitt, Physical Review B 2007, 75, 041102.
[29] R. Singh, I. A. I. Al-Naib, M. Koch, W. Zhang, Optics Express 2011, 19, 6312.
[30] C. Wu, A. B. Khanikaev, R. Adato, N. Arju, A. A. Yanik, H. Altug, G. Shvets, Nature Materials 2011, 11, 69.
[31] V. G. Kravets, F. Schedin, A. V. Kabashin, A. N. Grigorenko, Optics Letters 2010, 35, 956.
[32] S.-Q. Li, W. Zhou, D. Bruce Buchholz, J. B. Ketterson, L. E. Ocola, K. Sakoda, R. P. H. Chang, Applied Physics Letters 2014, 104, 231101.
[33] N. Meinzer, W. L. Barnes, I. R. Hooper, Nature Photonics 2014, 8, 889.
[34] B. D. Thackray, P. A. Thomas, G. H. Auton, F. J. Rodriguez, O. P. Marshall, V. G. Kravets, A. N. Grigorenko, Nano Letters 2015, 15, 3519.
[35] P. Zilio, M. Malerba, A. Toma, R. P. Zaccaria, A. Jacassi, F. D. Angelis, Nano Letters 2015, 15, 5200.
[36] A. Bitzer, J. Wallauer, H. Helm, H. Merbold, T. Feurer, M. Walther, Optics Express 2009, 17, 22108.
[37] P. Klarskov, A. T. Tarekegne, K. Iwaszczuk, X. C. Zhang, P. U. Jepsen, Scientific Reports 2016, 6, 37738.
[38] Q. Le-Van, E. Zoethout, E.-J. Geluk, M. Ramezani, M. Berghuis, J. Gómez Rivas, Advanced Optical Materials 2019, 7, 1801451.
[39] N. Xu, R. Singh, W. Zhang, Applied Physics Letters 2016, 109, 021108.
[40] C. T. Tan, E. Plum, R. Singh, Photonics 2019, 6, 75.
[41] J. Keller, C. Maissen, J. Haase, G. L. Paravicini-Bagliani, F. Valmorra, J. Palomo, J. Mangeney, J. Tignon, S. S. Dhillon, G. Scalari, J. Faist, Advanced Optical Materials 2017, 5, 1600884.
[42] M. Manjappa, Y. K. Srivastava, R. Singh, Physical Review B 2016, 94, 161103.
[43] T. C. Tan, Y. K. Srivastava, M. Manjappa, E. Plum, R. Singh, Applied Physics Letters 2018, 112, 201111.
[44] N. J. J. van Hoof, S. E. T. ter Huurne, R. H. J. Vervuurt, A. A. Bol, A. Halpin, J. Gómez Rivas, APL Photonics 2019, 4, 036104.
[45] A. Halpin, N. van Hoof, A. Bhattacharya, C. Mennes, J. Gomez Rivas, Physical Review B 2017, 96, 085110.
[46] M. C. Schaafsma, A. Bhattacharya, J. G. Rivas, ACS Photonics 2016, 3, 1596.
[47] N. Liu, H. Giessen, Angewandte Chemie International Edition 2010, 49, 9838.
[48] S. Zou, N. Janel, G. C. Schatz, The Journal of Chemical Physics 2004, 120, 10871.
[49] S. Zou, G. C. Schatz, Chemical Physics Letters 2005, 403, 62.
[50] J. H. Shi, E. Plum, V. A. Fedotov, N. I. Zheludev, in *Progress in Electromagnetics Research Symposium (PIERS 2011)*, 2011, 567.
[51] M. Manjappa, S.-Y. Chiam, L. Cong, A. A. Bettiol, W. Zhang, R. Singh, Applied Physics Letters 2015, 106, 181101.
[52] R. Singh, I. A. I. Al-Naib, Y. Yang, D. Roy Chowdhury, W. Cao, C. Rockstuhl, T. Ozaki, R. Morandotti, W. Zhang, Applied Physics Letters 2011, 99, 201107.
[53] A. E. Miroshnichenko, S. Flach, Y. S. Kivshar, Reviews of Modern Physics 2010, 82, 2257.